

Growth Mechanism and Thermal Stability of a MoS₂–Graphene Interface: A High-Resolution Core-Level Photoelectron Spectroscopy Study

Federico Loi, Luca Sbuelz, Paolo Lacovig, Daniel Lizzit, Luca Bignardi,* Silvano Lizzit, and Alessandro Baraldi



Cite This: *J. Phys. Chem. C* 2020, 124, 20889–20897



Read Online

ACCESS |



Metrics & More

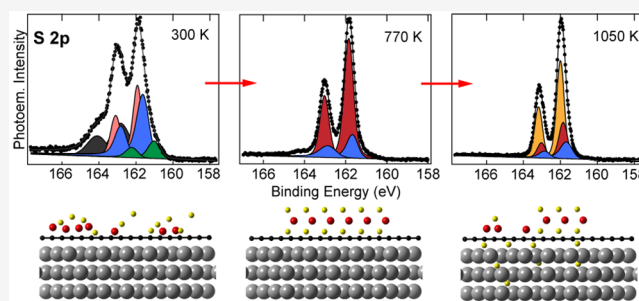


Article Recommendations



Supporting Information

ABSTRACT: We investigated the epitaxial growth of single-layer molybdenum disulfide (MoS₂) on graphene/Ir(111), aiming to understand its steps and mechanism and verify the stability of the heterostructure. By means of high-resolution X-ray photoelectron spectroscopy, we have revealed that accurate temperature control is crucial in allowing the formation and avoiding the degradation of single-layer MoS₂ on graphene. We observed that keeping the substrate temperature $T > 800$ K during the growth promotes efficient sulfur intercalation under graphene and the dissolution of sulfur in the Ir bulk, two processes that have been targeted as ones mainly responsible for irreversible degradation of the MoS₂ single layer on graphene. We believe that these results could be instrumental in understanding and improving the epitaxial growth protocols for the growth of heterostructures combining epitaxial graphene and transition-metal dichalcogenides.



INTRODUCTION

Molybdenum disulfide (MoS₂) is the most representative member of the family of semi-conducting transition-metal dichalcogenides (TMDCs). The electronic structure of this material is very peculiar since it shows a transition from an indirect to a direct band-gap semiconductor when downscaling it from bulk to a two-dimensional (2D) layer,^{1,2} a feature that makes this material very appealing for applications in nanoscaled optoelectronics and photonics. Moreover, due to the lack of inversion symmetry in the Brillouin zone, single-layer TMDCs such as MoS₂ and WS₂ have received considerable attention as they stand as ideal candidates to realize devices relying on the spin-valley degree of freedom.^{3–5} Besides the potential in new valley-based electronics, MoS₂ has been also actively studied as an efficient material in catalysis, in particular, in combination with titanium dioxide.^{6–11}

The possibility to combine different 2D materials in a van der Waals (vdW) heterostructure has paved the way to the realization of hybrid materials and new architectures whose properties can be tailored by a suitable choice and stacking of their elements.^{4,12–14} In the broad family of 2D materials, graphene (Gr) and MoS₂ are often coupled to form heterostructures. The initial step to form these structures is generally the mechanical cleaving of the 2D material from the parent bulk compound and the consequent stacking of the various elements on each other in the desired ordering.^{12–15} This top-down approach has the great advantage of producing

samples with outstanding quality but that are hardly scalable for industrially viable applications.

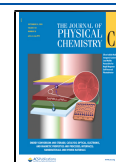
In order to overcome this bottleneck, as already successfully proven by the Gr-oriented research, several efforts have been devoted to develop epitaxial, bottom-up methods to grow 2D material-based heterostructures with a high degree of precision and tailored properties. In this framework, similar to chemical vapor deposition for Gr, it was possible to grow epitaxial MoS₂ whose features are strongly related to the substrate chosen for the growth. This is the case of single-layer TMDCs that can be epitaxially grown with a high degree of precision on noble-metal surfaces, such as Au(111)^{16–19} and Ag(111),^{20,21} making a step forward toward the exploitation of the complex spin texture of TMDCs on which the valleytronics concept relies.^{16,22,23}

The epitaxial growth of MoS₂–Gr heterostructures is of particular importance and oriented toward applications both in nanoscaled optoelectronics and catalysis since the employment of such a bottom-up method has been targeted as a reliable approach to assemble nanoarchitectures in an efficient and

Received: June 4, 2020

Revised: August 12, 2020

Published: September 1, 2020



reproducible way.^{24–30} An important issue to address when dealing with this growth method is the full understanding of the mechanism behind the formation of these heterostructures. This process can be considerably complex since several interdependent factors are involved in it (e.g., structural and electronic properties of the substrate, temperature, evaporation rate of the elemental species to form the TMDC layer). Furthermore, such knowledge is important since it is directly linked to the properties of the heterostructure and its stability. For example, it has been revealed by Hall et al.³¹ that the temperature of the substrate used during the growth has an important role in determining the degree of the azimuthal disorder of the final single layer for several TMDCs on Gr. Moreover, the choice of the substrate itself can play a capital role in defining the structural and electronic properties of the single-layer TMDC, which is important to consider when realizing heterostructures of this sort. For the epitaxial growth of single-layer MoS₂ on epitaxial Gr, this can be particularly relevant since the growth of MoS₂ requires usually the substrate to be heated and this could promote other processes such as the intercalation of the elemental species of MoS₂ under Gr.

Herein, we aim to investigate the formation mechanism of single-layer MoS₂ grown on epitaxial Gr on Ir(111), test its stability to temperature, and understand the causes of the degradation observed at high temperature. Epitaxial Gr/Ir(111) was used since it is a textbook example of a Gr–metal interface with a low density of defects, a moiré superlattice, and a weak Gr–substrate interaction.^{32–34} By employing an epitaxial growth protocol for MoS₂ on Gr already described in the literature,^{24–31} we have investigated the role played by the temperature in the formation of single-layer MoS₂ and its degradation, finding that the best temperature to obtain single-layer MoS₂ is approximately 800 K, a similar result to what has been obtained for epitaxial growth of MoS₂ on Au(111).¹⁶ Aiming to unravel the reasons of the degradation, we have observed that the Gr/Ir(111) interface is prone to S intercalation through the Gr defects, thus enabling the diffusion of sulfur on the Ir surface. Moreover, we were able to determine the formation of ordered adsorbate S structures on the Ir(111) surface, indicative of a strong interaction of S with the metal. Hence, we provide spectroscopic evidence that the intercalation of S under Gr and its dissolution in the Ir bulk during the growth participate in the degradation of the MoS₂ layer and identify these processes to be competing against the formation of the MoS₂ on Gr.

■ EXPERIMENTAL SECTION

The experiments were carried out in an ultrahigh-vacuum chamber of the photoemission end station of the SuperESCA beamline at the Elettra synchrotron radiation facility in Trieste, Italy. The base pressure during the experiments was ca. 1×10^{-10} mbar.

An Ir(111) single crystal was cleaned by cycles of Ar⁺ ion sputtering and annealing followed by exposure to oxygen (three temperature ramps up to 1080 K with a pressure of 2×10^{-7} mbar) and hydrogen (two temperature ramps up to 870 K with a pressure of 5×10^{-8} mbar). Gr was subsequently grown in situ on the surface by exposing the crystal to ethylene, according to a well-established protocol.^{34,35} The temperature of the sample was measured with a thermocouple in contact with the sample itself. Molybdenum was deposited on the

sample by employing a home-built Mo wire evaporator.^{16,21} A flux of sulfur atoms was obtained by heating a Knudsen cell containing FeS₂ kept at $T = 710$ K for a cumulative pressure inside the experimental chamber of ca. 7×10^{-9} mbar. In this work, a monolayer (ML) is defined as the surface density of iridium atoms per unit of area.

Core-level spectra were acquired using a SPECS Phoibos hemispherical electron energy analyzer (150 mm mean radius), equipped with electrostatic lenses and a microchannel plate-based delay-line detector developed at Elettra. The experimental setup combines high energy resolution with high data acquisition rates, thus allowing real-time monitoring of the evolution of the core-level spectral components during processes such as gas exposure and temperature ramps.³⁶ For the acquisition of the XPS spectra of the Ir 4f_{7/2}, Mo 3d, and S 2p core levels, a pass energy of 5 eV was used and a pass energy of 4 eV for the C 1s core levels. The measurements were performed with the photon beam impinging at the grazing incidence (70°), while photoelectrons were collected at a normal emission angle. The analysis area on the sample is determined by the dimension of the spot of the photon beam reaching the sample, which is smaller than $100 \times 10 \mu\text{m}^2$. The acquisition time of each spectrum is between 10 and 20 s, and the spectra during the annealing ramps were acquired while heating the sample. The temperature of the sample was measured with a K-type thermocouple spot-welded on the back of the Ir(111) crystal used as a substrate for the experiments.

The overall experimental energy resolution, which takes into account both the electron energy analyzer and the X-ray monochromator, was kept within 50 meV for measurements in the photon energy range of 200–400 eV. The core-level spectra were fitted with Doniach–Sunjic profiles³⁷ convoluted with a Gaussian function on a linear background, thus obtaining the lineshape parameters, the photoemission intensity, and core-level binding energies (BEs). The BE scale was aligned with the measured Fermi level of the Ir substrate. The comparison between photoemission intensities was performed considering the total area of each component. During the annealing, the lineshape and BE of each component were kept constant besides the Gaussian width, which was kept relaxed since it strongly depends on the temperature of the sample, because of phonon-induced core-level broadening. The low-energy electron diffraction (LEED) experiments were carried out using a commercial VG instrument with a transfer width of approximately 100 Å.

■ RESULTS AND DISCUSSION

Codeposition of Molybdenum and Sulfur. The initial step of our investigation was the study of the spectral features of the core levels measured during the growth of a single layer of MoS₂ on epitaxial Gr, which was obtained by codepositing molybdenum and sulfur on Gr/Ir(111) in a fashion similar to what was described earlier.^{24,31,38}

The growth of the single layer was achieved in two stages: an initial codeposition of Mo and S with the sample at room temperature followed by a second phase of annealing in a S flux. The process was monitored by XPS measurements of the Mo 3d and S 2p core levels. High-resolution XPS spectra acquired at the end of the first stage revealed a rich spectral composition for both signals (Figure 1a,b). In particular, the decomposition of the spectra showed four non-equivalent couples of components for the S 2p core level (Figure 1a) and

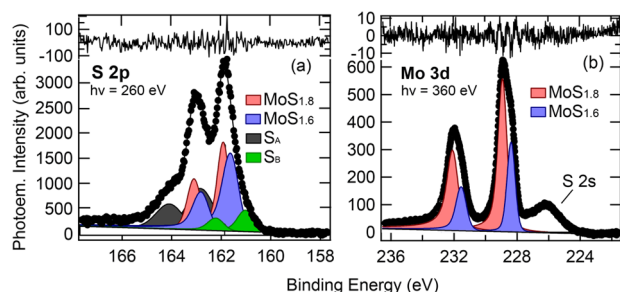


Figure 1. (a) XPS core-level S 2p and (b) Mo 3d spectra with their spectral components acquired with photons of energy $h\nu = 260$ eV and $h\nu = 360$ eV, respectively, after the codeposition of Mo and S at room temperature on Gr/Ir(111). Residuals are plotted at the top of each panel.

two non-equivalent couples for Mo 3d (Figure 1b) due to the spin–orbit splitting of 1.18 and 3.15 eV, respectively. Based on earlier reports,^{39,40} these outcomes can be interpreted by considering some of these components to have originated from Mo–S clusters having different degrees of Mo sulfidation with a MoS_x stoichiometry. The stoichiometric coefficient x linearly depends on the BE shift of Mo with respect to the BE of MoS_2 and the BE difference between Mo 3d and S 2p core levels of the same species. It was possible to assign the stoichiometric coefficients $\text{MoS}_{1.8}$ (red components with Mo 3d and S 2p having BEs of 228.92 and 161.94 eV, respectively) and $\text{MoS}_{1.6}$ (blue components with Mo 3d and S 2p having a BE of 228.38 and 161.64 eV, respectively) starting from the difference of BEs between Mo and the related S: 66.98 eV for the red components and 66.74 eV for the blue ones, which are indeed consistent with $x = 1.8 \pm 0.1$ and $x = 1.6 \pm 0.1$, respectively.³⁹ On the other hand, S_A (green peak at 161.03 eV) and S_B (gray peak at 162.90 eV) may represent sulfur atoms bound to other elements at the interface, such as carbon or iridium. These results are radically different from what has been observed for the growth of MoS_2 and WS_2 on the bare Au(111) surface^{16,17,38} where it appears that sulfur interacts only with molybdenum atoms. Therefore, the interaction between S not bound to Mo and the substrate seems to play an important role during the room-temperature growth of MoS_2 , meaning other adsorption processes competing with the formation of single-layer MoS_2 must be taken into account.

In the second stage, the sample was annealed in vacuum with a temperature ramp of 0.5 K/s from room temperature up to 1050 K in a sulfur-rich background ($P \approx 5 \times 10^{-8}$ mbar). XPS measurements of the Mo 3d and S 2p core levels acquired during the temperature ramp (Figure 2a,b) have shown an overall sharpening of the core-level spectra. While in a typical annealing experiment, one expects a broadening of both core-level components due to the phonon contribution, this narrowing can be ascribed to a reordering process of the system. The enhanced diffusion of the different atomic species has been proven effective in reordering the system and converting the partially reacted Mo–S species into MoS_2 .²⁴

We observed a variation in the spectral weight both for Mo 3d and S 2p in the temperature range of 400–600 K. The majority of the spectral components observed at the end of phase 1 (in particular, $\text{MoS}_{1.8}$) drastically lost their intensity. At the same time, two new components of Mo (purple, at 228.84 eV) and S (purple, at 161.85 eV) grew significantly in intensity (Figure 2c,d), and they clearly appear in the core-level spectra acquired at 770 K, as reported in Figure 3. It is

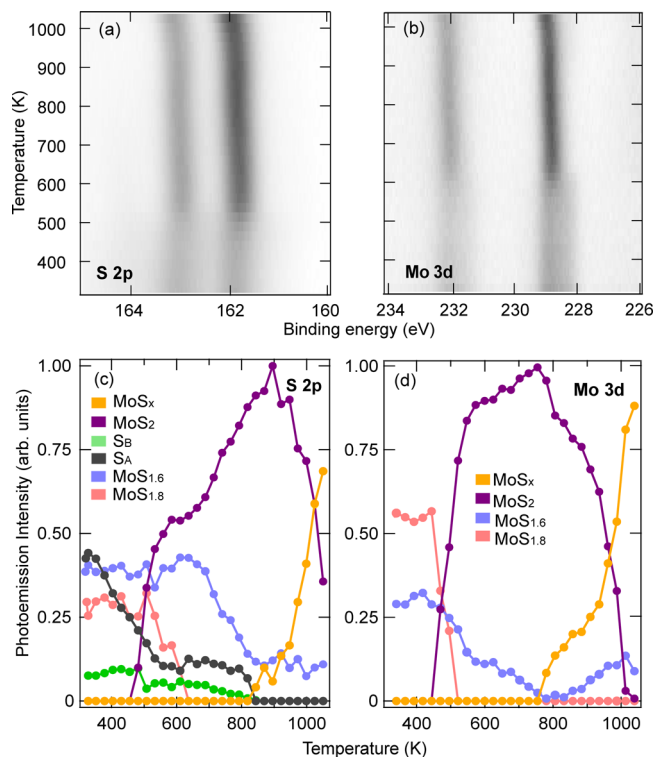


Figure 2. Time-resolved (a) S 2p and (b) Mo 3d spectra acquired during annealing in a sulfur background with a photon energy of $h\nu = 360$ eV. Temperature evolution of photoemission intensity of each spectral component of (c) S 2p and (d) Mo 3d.

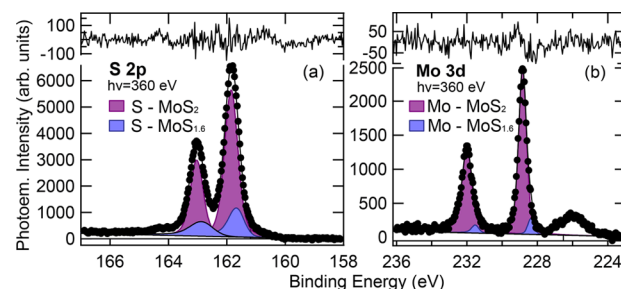


Figure 3. XPS spectra with the corresponding spectral decomposition for (a) S 2p and (b) Mo 3d measured at $T = 770$ K (photon energy $h\nu = 360$ eV). Residuals are plotted at the top of each panel.

significant to compare the position and lineshape of the Mo 3d and S 2p core levels that we obtained with the results observed for the growth of single-layer MoS_2 on Au(111).^{16,38,41} In the latter case, the transition to ordered single-layer MoS_2 was characterized by a consistent shift of the spectral weight toward a higher BE both for Mo 3d and S 2p, which is not happening here: the new S and Mo components have respectively BEs of 90 and 80 meV lower than the $\text{MoS}_{1.8}$ components.

The lineshape of the new components allows us to assign them to MoS_2 . The Lorentzian contribution to the overall linewidth of Mo 3d (0.23 eV) is in fact equal to that one obtained for MoS_2 on Au(111). The asymmetry parameter, which is related to the electron–hole excitation probability, is smaller on Gr than on Au(111) (compatible with 0 on Gr and 0.05 on Au(111)). This is connected to a modified electron density of states at the Fermi level, which is expected to be lower on Gr than on a bare metal such as Au(111). In addition to that, we observed that the S 2p spectrum does not display a

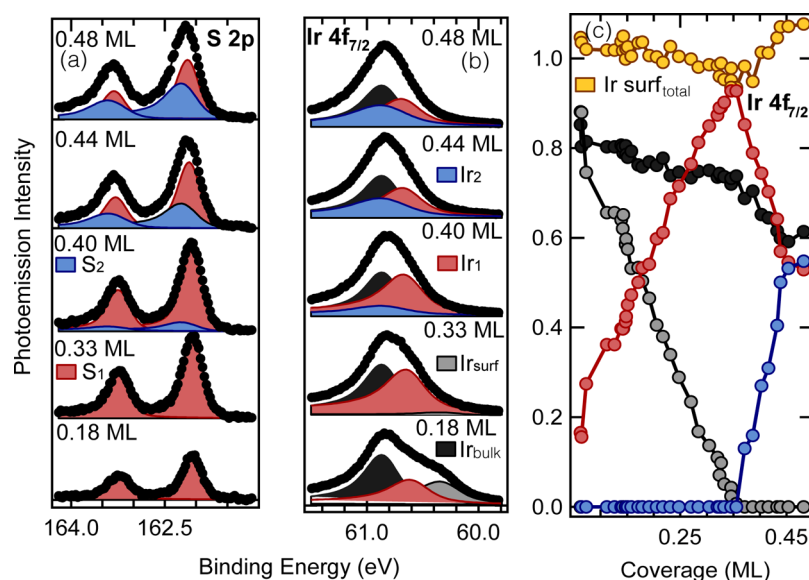


Figure 4. (a) Selected XPS core-level S 2p and (b) Ir 4f_{7/2} spectra for different coverage with their spectral decomposition. The spectra were acquired at room temperature with a photon energy $h\nu = 260$ eV. (c) Evolution of the photoemission intensity of each Ir 4f_{7/2} spectral component vs sulfur coverage.

second component at a higher BE for each of the peaks of the spin–orbit doublet as found in the case of MoS₂ grown on Au(111). The two components were associated to the upper and bottom layers of S in the MoS₂ structure.¹⁶ The lack of this feature can be attributed to the interaction of MoS₂ with the Gr substrate, which we expect to be weaker than the one between sulfur and gold. The result of this difference is that the lower and upper layers of sulfur in the MoS₂ single-layer structure are spectroscopically equivalent, showing the same BE and a similar lineshape. Last, a larger Gaussian width for the components of this interface can be explained to be due to a reduced overall degree of ordering with respect to the Au(111) case with a possible presence of several domain boundaries.

The behavior of the interface versus temperature was also investigated, in order to individuate the ideal temperature to promote the MoS₂ growth, hindering other unwanted species, and to test the stability of the interface. It is that, evident by plotting the intensity of the various spectral components versus temperature as shown in Figure 2c,d, the MoS₂ components reach the highest intensity between 750 and 800 K, which can be then considered as the ideal temperature range for the formation of MoS₂ over epitaxial Gr. This temperature seems to be lower than the one reported by Hall et al.³¹ via STM and LEED measurements for which the highest quality MoS₂ was obtained with annealing up to 1050 K. Our results suggest that, at ca. 800 K, the MoS₂ single layer starts to degrade as indicated by a sharp decrease in intensity of MoS₂ components (see Figure 2c,d) and by the appearance of two new components (yellow, with a BE of 228.94 eV and 162.00 eV for Mo 3d and S 2p) located at a higher BE. This temperature threshold is, on the other hand, an interesting analogy with the growth on Au(111) for which 800 K is the temperature needed to obtain MoS₂ of the highest quality possible. In the next paragraph, we will investigate the reasons behind this low degradation temperature when compared with the values reported by Hall et al.³¹ In particular, a possible cause of this different behavior could be due to a different sulfur flux reaching the sample because of the different geometries of the

experimental chambers. Hall et al.³¹ observed a tendency of sulfur atoms to leave the sample during annealing because of a lower residence time τ of unreacted sulfur on Gr compared to molybdenum. Additionally, they compared MoS₂ growth with different sulfur pressures (P_{sulfur}^a) during the annealing phase and observed that the system results to be very sensitive to this parameter. A too low P_{sulfur}^a leads to the formation of what they interpreted to be metallic Mo as a result of MoS₂ degradation. If a too high P_{sulfur}^a is used, on the other hand, it causes the formation of a second MoS₂ layer. The BE of the Mo component that we measured at a high temperature seems to point toward the first scenario, with the molybdenum atoms reverting back to the partially sulfided state MoS_x with $x \approx 1.8$ (a Δ BE between S and Mo components of 66.94 eV) after the bond with some sulfur atoms is broken.

Stimulated by the results about the thermally induced degradation of the MoS₂ layer, we endeavored to understand its causes for temperatures above 800 K. We supposed that the desorption and/or intercalation under Gr of one of the deposited species is an important actor in the phenomenon. To investigate this process more in detail, we performed two separate experiments: an uptake of atomic S on Ir(111) at room temperature and a deposition of S on Gr/Ir(111) at room temperature and during a temperature ramp, equivalent to the one used during the second phase of MoS₂ growth. The first experiment was instrumental to understand the strength of the interaction between S and the Ir(111) substrate. A strong interaction could cause, after a temperature-promoted intercalation of S under Gr, bonding of sulfur with iridium rather than with molybdenum atoms during the MoS₂ growth. On the contrary, such a process does not happen when depositing S on Au(111) since the interaction between sulfur and gold is known to be very weak.^{16,38,41} The second experiment was instead devised to understand whether S intercalates under Gr in the system Gr/Ir(111) and to identify the temperature at which S atoms leave the surface.

Role of the S–Ir(111) Interaction. The study on the S uptake on an Ir(111) surface was performed acquiring XPS core-level S 2p and Ir 4f_{7/2} spectra in real time during the

deposition. The decomposition of the S 2p spectra at different coverages is presented in Figure 4a. At the beginning of the process, only one spin–orbit doublet is observed (S_1 , red) with a BE of 162.04 eV for the S $2p_{3/2}$ component. In parallel with the increasing amount of sulfur deposited on the surface, we could see a shift of the spectral weight toward a higher BE, which is caused by the growth of a new couple of components (S_2 , blue) for a S coverage $\Theta > 0.33$ ML. The BE of the $2p_{3/2}$ component of S_2 is 162.18 eV. At the end of the uptake, the two S components have the same photoemission intensity. This spectral weight shift is a first indication of a change in the local environment around the adsorbed sulfur atoms. Together with the growth of the second component S_2 , we measured also a shift of the S_1 component toward a higher BE, which at the end of the experiment is 162.12 eV (for a S coverage $\theta \approx 0.5$ ML).

In order to understand the origin of the spectral weight shift from S_1 to S_2 , we acquired also the Ir $4f_{7/2}$ core-level spectra during the S exposure, as reported in Figure 4b. At the early stages of the uptake, we could individuate three distinct components: one corresponding to bulk iridium atoms (black), one to bare iridium surface atoms (Ir_{surf} , gray),⁴² and one to surface iridium bound to the adsorbed sulfur (Ir_1 , red) with a BE shift of +240 meV with respect to the surface component. In the coverage range $\Theta = 0$ –0.33, the BE shift of the third component was gradually shifted up to +340 meV with respect to the surface component. At a coverage $\Theta > 0.33$ ML, we also detected a fourth component (Ir_2 , blue) with a BE shift of +530 meV with respect to the clean surface. This new component represents the iridium surface atoms bonded to the S_2 sulfur species. At the end of the uptake, Ir_1 and Ir_2 present similar photoemission intensity (Figure 4c).

It has been reported that sulfur adsorbed on Ir(111) forms a $(\sqrt{3} \times \sqrt{3})R30^\circ$ ordered structure with only threefold fcc adsorption sites for $\Theta = 0.33$ ^{43–45} and a $c(4 \times 2)$ structure for $\Theta = 0.50$ ML.⁴⁶ The latter structure displays S in hcp and fcc adsorption sites with half of the Ir surface atoms bonded to one S adatom and the other half bonded to two S adatoms. This is accompanied by an adsorbate-induced rearrangement of the surface atoms with respect to the bare-surface situation, namely, the buckling of some surface atoms. In order to verify the compatibility of our outcomes with the results reported in the literature, we refer to earlier work indicating that the adsorbate-induced core-level shift of the clean surface component for a transition metal (TM) surface depends, in the first instance, both on the substrate geometry/symmetry and adsorption site.^{47,48} Assuming that, in our experiment, the $(\sqrt{3} \times \sqrt{3})R30^\circ$ structure is responsible for the Ir_1 and S_1 components, we can deduce that the adsorption site of S for the high-coverage configuration related to the Ir_2 component whose BE shift $\Delta E_{Ir_2} = 540$ meV is compatible with the configuration having a threefold adsorption site with a double-sulfur coordination for the Ir atoms, which is the configuration that was indeed identified and proposed for this interface.⁴⁶ A more detailed analysis of this adsorption process is provided in the Supporting Information.

The compatibility of our results with the literature was instrumental to establish the configuration as a function of sulfur coverage, which was calculated from the assumption that, for low coverage, the adsorption takes place on threefold sites with each Ir surface atom coordinated to one S adatom.^{43–45} As a preliminary constraint, we assume that the

Ir_{surf} component decreases linearly with respect to the S coverage with a slope of $m = -3$ (Figure 4c) as long as the Ir_2 component is not present (i.e., low-coverage conditions) since each atom of sulfur adsorbed onto a threefold site will cause the BE shift of three Ir surface atoms, turning them to Ir_1 . The coverage has then to be normalized to modify the abscissa's axis (representing the S coverage) and the slope of the Ir_{surf} curve until the slope $m = -3$ is reached. Based on these assumptions, we obtained the final coverage of S atoms on the Ir(111) surface, which was calculated to be $\Theta = 0.48 \pm 0.05$ ML.

A LEED pattern was acquired at the end of the S uptake, and it confirmed the $c(4 \times 2)$ ordering (see the Supporting Information). This and the XPS analysis we performed are in line with the surface model proposed by Pielic et al.⁴⁶ The formation of highly ordered structures in this experiment indicates a strong interaction between sulfur and the Ir(111) substrate, which could interfere with the MoS_2 growth by hindering some sulfur atoms from bonding to molybdenum atoms on Gr.

Disrupting the Growth: Intercalation of S at the Gr/Ir(111) Interface. The next step to understand the behavior of sulfur in the MoS_2 growth process is the study of intercalation of sulfur at the Gr/Ir(111) interface, which could be a competing process of the MoS_2 growth. We have analyzed the behavior of the Ir $4f_{7/2}$ core level acquired via XPS exposing Gr/Ir(111) to a partial pressure of atomic sulfur of up to 6×10^{-8} mbar for 45 min with the substrate at room temperature. The spectrum at the beginning of the deposition (Figure 5a, bottom) shows the same spectral components

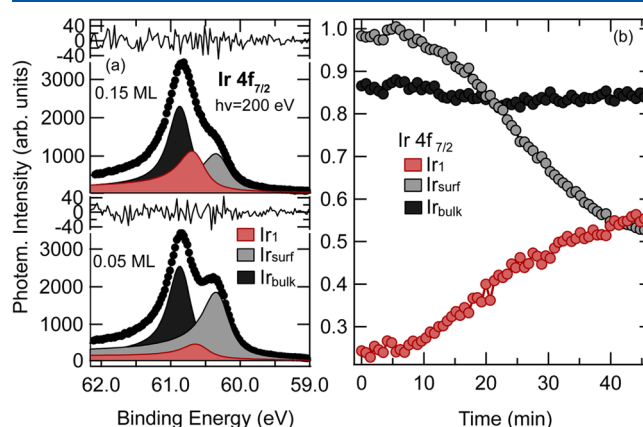


Figure 5. (a) XPS spectra and decomposition of Ir $4f_{7/2}$ core level before (bottom) and after (top) a 45 min exposure to sulfur. (b) Evolution of the photoemission intensity of each Ir $4f_{7/2}$ spectral component vs time during sulfur exposure.

revealed in the previous paragraph: one associated with the bulk Ir atoms (black), another with the first-layer clean Ir atoms (Ir_{surf} , gray), and a third component (Ir_1 , red) indicating a small contamination of sulfur. After the deposition (Figure 5a, top), the clean surface component was strongly reduced in favor of Ir_1 while the bulk component remained unchanged.

The different behaviors of Ir_{surf} , Ir_1 , and Ir_{bulk} are better highlighted in Figure 5b in which we plot the photoemission intensity of the three different components measured via XPS during the deposition. During the first 8 min, with a partial sulfur pressure of approximately 10^{-9} mbar, the photoemission intensity of all the components is constant. After the S partial

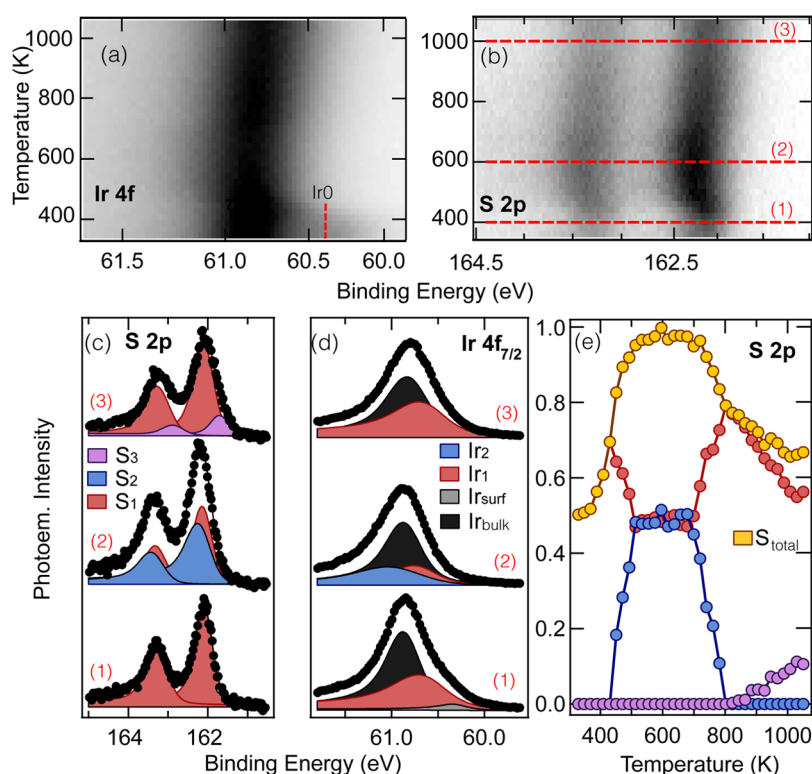


Figure 6. (a) Time-resolved Ir $4f_{7/2}$ with the Ir_{surf} binding energy highlighted and (b) S 2p spectrum acquired during annealing in the sulfur background. (c) Selected spectra of S 2p and (d) Ir $4f_{7/2}$ are plotted with their spectral decomposition at different stages of the experiment. (e) Evolution of the photoemission intensity of each spectral component of the S 2p core level and their sum. Both core levels were acquired with $h\nu = 260$ eV.

pressure was slightly increased to 10^{-8} mbar, the Ir_{surf} component starts decreasing. On the other hand, Ir₁ increases at the expense of Ir_{surf} while the photoemission intensity of the bulk component only slightly decreases because of the screening due to adsorbed S atoms. The fact that Ir₁ decreases faster than the bulk component indicates that Ir surface atoms are interacting with an adsorbate. Consequently, we deduced that some sulfur is intercalating under the Gr and is being adsorbed on the iridium surface, causing the shift of spectral weight from Ir_{surf} toward Ir₁. If the decreasing of the photoemission intensity of Ir_{surf} was caused by other effects such as screening due to sulfur atoms adsorbed on Gr, then also the bulk component would have the same behavior, which is not the case. The fact that we have intercalation already at room temperature is interesting and not common in the case of Gr, for which the temperature usually necessary to promote and achieve the intercalation of atoms under a complete layer of Gr is of the order of at least 400 K.^{35,49–52} In particular, this is quite different from what was recently reported⁴⁶ where the temperature to initiate the S intercalation under graphene is 450 K.

In the end, we performed an annealing of the same sample simulating the conditions used for the growth of MoS₂, i.e., a temperature ramp of 0.5 K/s up to 1050 K in a 5×10^{-8} mbar background of sulfur. The behavior of the intensity of the Ir $4f_{7/2}$ core level reported in Figure 6a shows how the clean-surface component completely disappears at $T = 400$ K, indicating a strong intercalation of sulfur under Gr, which causes the surface to be completely covered by sulfur atoms. For $T > 400$ K, we registered a shift in the S 2p spectral weight toward a higher BE (Figure 6b). From the decomposition of

the S 2p core-level spectra acquired during the annealing ramp (Figure 6c) and the behavior of the photoemission intensity of each component in Figure 6e, it is possible to see how, at first, only one couple of sulfur components (S₁, red at 162.08 eV) was present, having the same lineshape detected for the adsorption of S on bare Ir(111). At $T = 400$ K, because of the strong intercalation observed in Figure 6a, the overall S 2p photoemission intensity starts increasing. At first, only the S₁ component increases, but then a second component (S₂, blue at 162.18 eV) starts growing, partially replacing S₁. The behavior of S₁ and S₂ is the same as what is reported in the previous paragraph: the transition from S₁ to S₂ can be interpreted as the result of a change in the adsorption site caused by different sulfur coverages on the Ir(111) surface. This analysis indicates that the structure formed by the sulfur adatoms on the iridium surface under Gr is the same as the one obtained during the S uptake on clean Ir. The intensity of S₂ reaches a saturation value at ca. $T = 500$ K, and the system appears to be stable up to ca. $T = 700$ K with S₁ and S₂ showing the same photoemission intensity. This suggests that the two inequivalent species have the same abundance on the surface. While the S components in this temperature range have the same BE as those stated in the previous paragraph, the Ir₂ component in the Ir $4f_{7/2}$ core-level spectra (Figure 6d) has a BE of 100 meV higher than that of the same component of the previous experiment. We speculate that this could have been caused by a different degree of surface buckling of Ir atoms and/or a possible increased interaction of lifted Ir atoms with Gr.

A new phase of the annealing experiment can be observed at 700 K: the stability of the system is broken, and the total

coverage starts decreasing, causing a complete transition back from S_2 to S_1 . This could mean that we are reverting to a low-coverage structure as sulfur atoms start leaving the surface. S_2 is completely vanished at 800 K. Above this temperature, a third component arises (S_3 , purple at 161.68 eV), and it keeps increasing until the end of the annealing ramp. The total sulfur intensity of the S 2p components (orange in Figure 6e) begins to decrease for $T > 700$ K. This is indicative of sulfur leaving the sample surface, either by desorption or penetration into the iridium bulk as already speculated in previous studies for the adsorption on Pt(111)⁵³ and Pd(111),⁵⁴ which are surfaces electronically and structurally similar to Ir(111). This last hypothesis can explain the presence of the new component S_3 , which could be generated by the sulfur atoms that penetrated into the iridium bulk. Moreover, in the Ir 4f_{7/2} spectra at high temperature, we observed a BE shift of the bulk component of 100 meV toward a lower BE, indicating a possible bonding of subsurface Ir atoms to S.

We found that the temperature at which the amount of S on the surface starts decreasing (~ 750 K) is very similar to the temperature corresponding to the degradation of MoS_2 we previously reported. We suggest that there is a link between the two phenomena: S desorption and/or intercalation under Gr and ultimately the diffusion into the bulk crystal may play an important role in the degradation of MoS_2 . Interestingly, the S_3 component disappears when the sample is cooled to room temperature and the photoemission intensity of the overall sulfur reverts back to the saturation value, indicating a surface segregation at the Gr/Ir interface (see the Supporting Information).

CONCLUSIONS

We have characterized by core-level photoemission spectroscopy the process of epitaxial growth of a single layer of MoS_2 at a Gr/Ir(111) interface, revealing how thermal annealing under a S flux causes the transition from partially sulfided Mo clusters, obtained by co-evaporating S and Mo on a substrate at RT, to a single layer of MoS_2 . The temperature at which this process takes place is approximately 800 K; above which, we observed a degradation of the MoS_2 layer with a loss of S from the surface. Additional experiments allowed to disentangle the role of the different parameters and atomic species in the growth process. In particular, the experiments of adsorption of S on the bare Ir(111) surface revealed that there is a strong interaction between the sulfur and the metal unlike what happens for a direct growth of MoS_2 on Au(111). Furthermore, we proved that Gr/Ir(111) is rather prone to intercalation of S under Gr. This process is competing against the formation of MoS_2 already at room temperature since the sulfur atoms that diffuse on the Gr surface and penetrate under it cannot bind with molybdenum atoms to form MoS_2 . The results we have herein described have cast light on the mechanism of formation and degradation of MoS_2 on epitaxial Gr, evidencing the important role played by the temperature and intercalation. We believe that the findings we report could be extended to the epitaxial growth of other TMDC-based heterostructures, aiming to improve their quality and stability and understand their potential in technology-oriented applications.

ASSOCIATED CONTENT

Supporting Information

The Supporting Information is available free of charge at <https://pubs.acs.org/doi/10.1021/acs.jpcc.0c05037>.

Details about the adsorption of S on Ir(111) and additional XPS spectra (PDF)

AUTHOR INFORMATION

Corresponding Author

Luca Bignardi – Department of Physics, University of Trieste, Trieste 34127, Italy; orcid.org/0000-0002-9846-9100; Email: lbignardi@units.it

Authors

Federico Loi – Department of Physics, University of Trieste, Trieste 34127, Italy

Luca Sbuelz – Department of Physics, University of Trieste, Trieste 34127, Italy

Paolo Lacovig – Elettra - Sincrotrone Trieste, Trieste 34149, Italy; orcid.org/0000-0001-7001-7930

Daniel Lizzit – Elettra - Sincrotrone Trieste, Trieste 34149, Italy

Silvano Lizzit – Elettra - Sincrotrone Trieste, Trieste 34149, Italy; orcid.org/0000-0003-1620-7228

Alessandro Baraldi – Department of Physics, University of Trieste, Trieste 34127, Italy; Elettra - Sincrotrone Trieste, Trieste 34149, Italy; IOM-CNR, Laboratorio TASC, 34149 Trieste, Italy; orcid.org/0000-0001-5690-9668

Complete contact information is available at:

<https://pubs.acs.org/doi/10.1021/acs.jpcc.0c05037>

Notes

The authors declare no competing financial interest.

REFERENCES

- (1) Splendiani, A.; Sun, L.; Zhang, Y.; Li, T.; Kim, J.; Chim, C.-Y.; Galli, G.; Wang, F. Emerging Photoluminescence in Monolayer MoS_2 . *Nano Lett.* **2010**, *10*, 1271–1275.
- (2) Mak, K. F.; Lee, C.; Hone, J.; Shan, J.; Heinz, T. F. Atomically Thin MoS_2 : A New Direct-Gap Semiconductor. *Phys. Rev. Lett.* **2010**, *105*, 136805.
- (3) Mak, K. F.; Xiao, D.; Shan, J. Light-valley interactions in 2D semiconductors. *Nat. Photonics* **2018**, *12*, 451–460.
- (4) Mak, K. F.; Shan, J. Opportunities and challenges of interlayer exciton control and manipulation. *Nat. Nanotechnol.* **2018**, *13*, 974–976.
- (5) Schaibley, J. R.; Yu, H.; Clark, G.; Rivera, P.; Ross, J. S.; Seyler, K. L.; Yao, W.; Xu, X. Valleytronics in 2D materials. *Nat. Rev. Mater.* **2016**, *1*, 16055.
- (6) Chen, B.; Meng, Y.; Sha, J.; Zhong, C.; Hu, W.; Zhao, N. Preparation of $\text{MoS}_2/\text{TiO}_2$ based nanocomposites for photocatalysis and rechargeable batteries: progress, challenges, and perspective. *Nanoscale* **2017**, *10*, 34–68.
- (7) Han, B.; Hu, Y. H. MoS_2 as a co-catalyst for photocatalytic hydrogen production from water. *Energy Sci. Eng.* **2016**, *4*, 285–304.
- (8) He, H.; Lin, J.; Fu, W.; Wang, X.; Wang, H.; Zeng, Q.; Gu, Q.; Li, Y.; Yan, C.; Tay, B. K.; et al. $\text{MoS}_2/\text{TiO}_2$ Edge-On Heterostructure for Efficient Photocatalytic Hydrogen Evolution. *Adv. Energy Mater.* **2016**, *6*, 1600464.
- (9) Kim, J.; Byun, S.; Smith, A. J.; Yu, J.; Huang, J. Enhanced Electrocatalytic Properties of Transition-Metal Dichalcogenides Sheets by Spontaneous Gold Nanoparticle Decoration. *J. Phys. Chem. Lett.* **2013**, *4*, 1227–1232.
- (10) Xiang, Q.; Yu, J.; Jaroniec, M. Synergetic Effect of MoS_2 and Graphene as Cocatalysts for Enhanced Photocatalytic H_2 Production

Activity of TiO₂ Nanoparticles. *J. Am. Chem. Soc.* **2012**, *134*, 6575–6578.

(11) Zhou, W.; Yin, Z.; Du, Y.; Huang, X.; Zeng, Z.; Fan, Z.; Liu, H.; Wang, J.; Zhang, H. Synthesis of Few-Layer MoS₂ Nanosheet-Coated TiO₂ Nanobelt Heterostructures for Enhanced Photocatalytic Activities. *Small* **2013**, *9*, 140–147.

(12) Geim, A. K.; Grigorieva, I. V. Van der Waals heterostructures. *Nature* **2013**, *499*, 419–425.

(13) Novoselov, K. S.; Mishchenko, A.; Carvalho, A.; Neto, A. H. C. 2D materials and van der Waals heterostructures. *Science* **2016**, *353*, No. aac9439.

(14) Liang, S.-J.; Cheng, B.; Cui, X.; Miao, F. Van der Waals Heterostructures for High-Performance Device Applications: Challenges and Opportunities. *Adv. Mater.* **2019**, 1903800.

(15) Wang, L.; Hu, P.; Long, Y.; Liu, Z.; He, X. Recent advances in ternary two-dimensional materials: synthesis, properties and applications. *J. Mater. Chem. A* **2017**, *5*, 22855–22876.

(16) Bana, H.; Travaglia, E.; Bignardi, L.; Lacovig, P.; Sanders, C. E.; Dendzik, M.; Michiardi, M.; Bianchi, M.; Lizzit, D.; Presel, F.; et al. Epitaxial growth of singleorientation high-quality MoS₂ monolayers. *2D Mater.* **2018**, *5*, 035012.

(17) Bignardi, L.; Lizzit, D.; Bana, H.; Travaglia, E.; Lacovig, P.; Sanders, C. E.; Dendzik, M.; Michiardi, M.; Bianchi, M.; Ewert, M.; et al. Growth and structure of singly oriented single-layer tungsten disulfide on Au(111). *Phys. Rev. Mater.* **2019**, *3*, No. 014003.

(18) Arnold, F.; Stan, R.-M.; Mahatha, S. K.; Lund, H. E.; Curcio, D.; Dendzik, M.; Bana, H.; Travaglia, E.; Bignardi, L.; Lacovig, P.; et al. Novel single-layer vanadium sulphide phases. *2D Mater.* **2018**, *5*, No. 045009.

(19) Stan, R.-M.; Mahatha, S. K.; Bianchi, M.; Sanders, C. E.; Curcio, D.; Hofmann, P.; Miwa, J. A. Epitaxial single-layer NbS₂ on Au(111): Synthesis, structure, and electronic properties. *Phys. Rev. Mater.* **2019**, *3*, No. 044003.

(20) Dendzik, M.; Bruix, A.; Michiardi, M.; Ngankou, A. S.; Bianchi, M.; Miwa, J. A.; Hammer, B.; Hofmann, P.; Sanders, C. E. Substrate-induced semiconductor-to-metal transition in monolayer WS₂. *Phys. Rev. B* **2017**, *96*, 235440.

(21) Volckaert, K.; Rostami, H.; Biswas, D.; Marković, I.; Andreatta, F.; Sanders, C. E.; Majchrzak, P.; Cacho, C.; Chapman, R. T.; Wyatt, A.; et al. Momentum-resolved linear dichroism in bilayer MoS₂. *Phys. Rev. B* **2019**, *100*, 241406.

(22) Eickholt, P.; Sanders, C.; Dendzik, M.; Bignardi, L.; Lizzit, D.; Lizzit, S.; Bruix, A.; Hofmann, P.; Donath, M. Spin Structure of K Valleys in Single-Layer WS₂ on Au(111). *Phys. Rev. Lett.* **2018**, *121*, 136402.

(23) Beyer, H.; Rohde, G.; Grubišić Čabo, A.; Stange, A.; Jacobsen, T.; Bignardi, L.; Lizzit, D.; Lacovig, P.; Sanders, C. E.; Lizzit, S.; et al. 80% Valley Polarization of Free Carriers in Singly Oriented Single-Layer WS₂ on Au(111). *Phys. Rev. Lett.* **2019**, *123*, 236802.

(24) Miwa, J. A.; Dendzik, M.; Grønborg, S. S.; Bianchi, M.; Lauritsen, J. V.; Hofmann, P.; Ulstrup, S. Van der Waals Epitaxy of Two-Dimensional MoS₂-Graphene Heterostructures in Ultrahigh Vacuum. *ACS Nano* **2015**, *9*, 6502–6510.

(25) Bertolazzi, S.; Krasnozhan, D.; Kis, A. Nonvolatile Memory Cells Based on MoS₂/Graphene Heterostructures. *ACS Nano* **2013**, *7*, 3246–3252.

(26) Ebnonnasir, A.; Narayanan, B.; Kodambaka, S.; Ciobanu, C. V. Tunable MoS₂ bandgap in MoS₂-graphene heterostructures. *Appl. Phys. Lett.* **2014**, *105*, No. 031603.

(27) Huang, Z.; Han, W.; Tang, H.; Ren, L.; Chander, D. S.; Qi, X.; Zhang, H. Photoelectrochemical-type sunlight photodetector based on MoS₂/graphene heterostructure. *2D Mater.* **2015**, *2*, No. 035011.

(28) Pierucci, D.; Henck, H.; Avila, J.; Balan, A.; Naylor, C. H.; Patriarche, G.; Dappe, Y. J.; Silly, M. G.; Sirotti, F.; Johnson, A. T. C.; et al. Band Alignment and Minigaps in Monolayer MoS₂-Graphene van derWaals Heterostructures. *Nano Lett.* **2016**, *16*, 4054–4061.

(29) Toth, P. S.; Velický, M.; Bissett, M. A.; Slater, T. J. A.; Savjani, N.; Rabiou, A. K.; Rakowski, A. M.; Brent, J. R.; Haigh, S. J.; O'Brien, P.; et al. Asymmetric MoS₂/Graphene/Metal Sandwiches: Prepara-

tion, Characterization, and Application. *Adv. Mater.* **2016**, *28*, 8256–8264.

(30) Zhao, G.; Hou, J.; Wu, Y.; He, J.; Hao, X. Preparation of 2D MoS₂/Graphene Heterostructure through a Monolayer Intercalation Method and its Application as an Optical Modulator in Pulsed Laser Generation. *Adv. Opt. Mater.* **2015**, *3*, 937–942.

(31) Hall, J.; Pielic, B.; Murray, C.; Jolie, W.; Wekking, T.; Busse, C.; Kralj, M.; Michely, T. Molecular beam epitaxy of quasi-freestanding transition metal disulphide monolayers on van der Waals substrates: a growth study. *2D Mater.* **2018**, *5*, No. 025005.

(32) Coraux, J.; N'Diaye, A. T.; Busse, C.; Michely, T. Structural coherency of graphene on Ir(111). *Nano Lett.* **2008**, *8*, 565–570.

(33) Coraux, J.; N'Diaye, A. T.; Engler, M.; Busse, C.; Wall, D.; Buckanie, N.; zu Heringdorf, F.-J. M.; van Gestel, R.; Poelsema, B.; Michely, T. Growth of graphene on Ir(111). *New J. Phys.* **2009**, *11*, No. 023006.

(34) Presel, F.; Tetlow, H.; Bignardi, L.; Lacovig, P.; Tache, C. A.; Lizzit, S.; Kantorovich, L.; Baraldi, A. Graphene growth by molecular beam epitaxy: an interplay between desorption, diffusion and intercalation of elemental C species on islands. *Nanoscale* **2018**, *10*, 7396–7406.

(35) Larciprete, R.; Ulstrup, S.; Lacovig, P.; Dalmiglio, M.; Bianchi, M.; Mazzola, F.; Hornekær, L.; Orlando, F.; Baraldi, A.; Hofmann, P.; et al. Oxygen Switching of the Epitaxial Graphene–Metal Interaction. *ACS Nano* **2012**, *6*, 9551–9558.

(36) Baraldi, A.; Comelli, G.; Lizzit, S.; Kiskinova, M.; Paolucci, G. Real-time X-ray photoelectron spectroscopy of surface reactions. *Surf. Sci. Rep.* **2003**, *49*, 169–224.

(37) Doniach, S.; Sunjic, M. Many-electron singularity in X-ray photoemission and X-ray line spectra from metals. *J. Phys. C: Solid State Phys.* **1970**, *3*, 285–291.

(38) Bruix, A.; Fuchtbauer, H. G.; Tuxen, A. K.; Walton, A. S.; Andersen, M.; Porsgaard, S.; Besenbacher, F.; Hammer, B.; Lauritsen, J. V. In Situ Detection of Active Edge Sites in Single-Layer MoS₂ Catalysts. *ACS Nano* **2015**, *9*, 9322–9330.

(39) Baker, M. A.; Gilmore, R.; Lenardi, C.; Gissler, W. XPS investigation of preferential sputtering of S from MoS₂ and determination of MoS_x stoichiometry from Mo and S peak positions. *Appl. Surf. Sci.* **1999**, *150*, 255–262.

(40) Lince, J. R.; Carre, D. J.; Fleischauer, P. D. Effects of argon-ion bombardment on the basal plane surface of molybdenum disulfide. *Langmuir* **1986**, *2*, 805–808.

(41) Bruix, A.; Lauritsen, J. V.; Hammer, B. Effects of particle size and edge structure on the electronic structure, spectroscopic features, and chemical properties of Au(111)-supported MoS₂ nanoparticles. *Faraday Discuss.* **2016**, *188*, 323–343.

(42) Bianchi, M.; Cassese, D.; Cavallin, A.; Comin, R.; Orlando, F.; Postregna, L.; Golfetto, E.; Lizzit, S.; Baraldi, A. Surface core level shifts of clean and oxygen covered Ir(111). *New J. Phys.* **2009**, *11*, No. 063002.

(43) Andersen, M.; Hornekær, L.; Hammer, B. Understanding intercalation structures formed under graphene on Ir(111). *Phys. Rev. B* **2014**, *90*, 155428.

(44) Krekelberg, W. P.; Greeley, J.; Mavrikakis, M. Atomic and Molecular Adsorption on Ir(111). *J. Phys. Chem. B* **2003**, *108*, 987–994.

(45) Chan, C.-M.; Weinberg, W. H. The structure of the ($\sqrt{3}\times\sqrt{3}$) R30° sulfur overlayer on the iridium (111) surface. *J. Chem. Phys.* **1979**, *71*, 3988–3990.

(46) Pielic, B.; Hall, J.; Despoja, V.; Rakić, I. Š.; Petrović, M.; Sohani, A.; Busse, C.; Michely, T.; Kralj, M. Sulfur Structures on Bare and Graphene-Covered Ir(111). *J. Phys. Chem. C* **2020**, *124*, 6659–6668.

(47) Baraldi, A.; Lizzit, S.; Comelli, G.; Kiskinova, M.; Rosei, R.; Honkala, K.; Nørskov, J. K. Spectroscopic Link between Adsorption Site Occupation and Local Surface Chemical Reactivity. *Phys. Rev. Lett.* **2004**, *93*, No. 046101.

(48) Baraldi, A. Structure and chemical reactivity of transition metal surfaces as probed by synchrotron radiation core level photoelectron spectroscopy. *J. Phys.: Condens. Matter* **2008**, *20*, No. 093001.

(49) Bignardi, L.; Lacovig, P.; Dalmiglio, M. M.; Orlando, F.; Ghafari, A.; Petaccia, L.; Baraldi, A.; Larciprete, R.; Lizzit, S. Key role of rotated domains in oxygen intercalation at graphene on Ni(111). *2D Mater.* **2017**, *4*, No. 025106.

(50) Ulstrup, S.; Lacovig, P.; Orlando, F.; Lizzit, D.; Bignardi, L.; Dalmiglio, M.; Bianchi, M.; Mazzola, F.; Baraldi, A.; Larciprete, R.; et al. Photoemission investigation of oxygen intercalated epitaxial graphene on Ru(0001). *Surf. Sci.* **2018**, *678*, 57–64.

(51) Presel, F.; Jabeen, N.; Pozzo, M.; Curcio, D.; Omiciuolo, L.; Lacovig, P.; Lizzit, S.; Alf , D.; Baraldi, A. Unravelling the roles of surface chemical composition and geometry for the graphene–metal interaction through C1s core-level spectroscopy. *Carbon* **2015**, *93*, 187–198.

(52) De Angelis, D.; Presel, N.; Jabeen, N.; Francesco, N.; Bignardi, L.; Lizzit, D.; Lacovig, P.; Lizzit, S.; Montini, T.; Fornasiero, P.; Alf , D.; Baraldi, A. Interfacial two-dimensional oxide enhances photocatalytic activity of graphene/titania via electronic structure modification. *Carbon* **2020**, *157*, 350–357.

(53) Heegemann, W.; Meister, K. H.; Bechtold, E.; Hayek, K. The adsorption of sulfur on the (100) and (111) faces of platinum; A LEED and AES study. *Surf. Sci.* **1975**, *49*, 161–180.

(54) B mermann, J.; Huck, M.; Kuntze, J.; Rauch, T.; Speller, S.; Heiland, W. An STM, AES and LEED study of the segregated sulfur on Pd(111). *Surf. Sci.* **1996**, *357-358*, 849–854.